

LA-UR- 98-3183


Approved for public release;
distribution is unlimited.

Title: Hot Blast Stove Process Model and
Model-Based Controller

CONF-980923--

Author(s): Muske, Ken-Villanova-XCM
Howse, James-XCM
Hansen, Glen-XCM
Cagliostro, Dominic-XCM
Chaubal, Pinakin-Research Laboratories

Submitted to: Association of Iron and Steel Engineers
Pittsburgh, PA
September 21, 1998

DISTRIBUTION OF THIS DOCUMENT IS UNLIMITED 

MASTER

Los Alamos
NATIONAL LABORATORY

Los Alamos National Laboratory, an affirmative action/equal opportunity employer, is operated by the University of California for the U.S. Department of Energy under contract W-7405-ENG-36. By acceptance of this article, the publisher recognizes that the U.S. Government retains a nonexclusive, royalty-free license to publish or reproduce the published form of this contribution, or to allow others to do so, for U.S. Government purposes. Los Alamos National Laboratory requests that the publisher identify this article as work performed under the auspices of the U.S. Department of Energy. The Los Alamos National Laboratory strongly supports academic freedom and a researcher's right to publish; as an institution, however, the Laboratory does not endorse the viewpoint of a publication or guarantee its technical correctness.

DISCLAIMER

This report was prepared as an account of work sponsored by an agency of the United States Government. Neither the United States Government nor any agency thereof, nor any of their employees, makes any warranty, express or implied, or assumes any legal liability or responsibility for the accuracy, completeness, or usefulness of any information, apparatus, product, or process disclosed, or represents that its use would not infringe privately owned rights. Reference herein to any specific commercial product, process, or service by trade name, trademark, manufacturer, or otherwise does not necessarily constitute or imply its endorsement, recommendation, or favoring by the United States Government or any agency thereof. The views and opinions of authors expressed herein do not necessarily state or reflect those of the United States Government or any agency thereof.

DISCLAIMER

Portions of this document may be illegible in electronic image products. Images are produced from the best available original document.

Hot Blast Stove Process Model and Model-Based Controller

Kenneth R. Muske
Department of Chemical Engineering
Villanova University
Villanova, PA 19085-1681

James W. Howse, Glen A. Hansen, and Dominic J. Cagliostro
Computational Science Methods Group
Los Alamos National Laboratory
Los Alamos, NM 87545

Pinakin C. Chaubal
Research Laboratories
Inland Steel Industries, Inc.
East Chicago, IN 46312

1 Introduction

This paper describes the process model and model-based control techniques implemented on the hot blast stoves for the No. 7 Blast Furnace at the Inland Steel facility in East Chicago, Indiana. A detailed heat transfer model of the stoves is developed and verified using plant data. This model is used as part of a predictive control scheme to determine the minimum amount of fuel necessary to achieve the blast air requirements. The model is also used to predict maximum and minimum temperature constraint violations within the stove so that the controller can take corrective actions while still achieving the required stove performance.

One of the major sources of energy for the blast furnace is the *sensible* heat coming from the preheated air, referred to as *blast air*, that is injected into the furnace. This air is preheated in tall, cylindrical, refractory-filled heat exchangers called hot blast stoves. Figure 1 presents a schematic of a hot blast stove at the Inland Steel facility. These stoves go through alternate cycles of heating and cooling referred to as 'on-gas' and 'on-blast' cycles respectively. During the

on-gas cycle, the stove is heated by the combustion of fuel gas in the combustion chamber of the stove. The combustion products, which are referred to as waste gas, enter the dome or top of the stove and then descend down through a checkerwork arrangement of refractory bricks referred to as the checkers. For the on-blast cycle, the flow through the stove is reversed. Air passes up through the checkers, where it is heated, into the dome, and then downward into the combustion chamber. The temperature of the blast air is controlled by diverting some of the cold blast air into the combustion chamber to mix with the heated air. The amount of cold blast air diverted is controlled using a by-pass valve. The combustion chamber is the chamber on the left in Figure 1. The chamber on the right contains the refractory brick or checkers. The insert in Brick Zone #2 shows the shape of one of the checkers.

The principal fuel for the hot blast stove is the carbon monoxide and hydrogen contained in the top gas coming from the blast furnace. In order to achieve the required blast air temperature, however, the top gas must be enriched with a higher heating value fuel. Natural gas is presently being used at the East Chicago facility. The key to re-

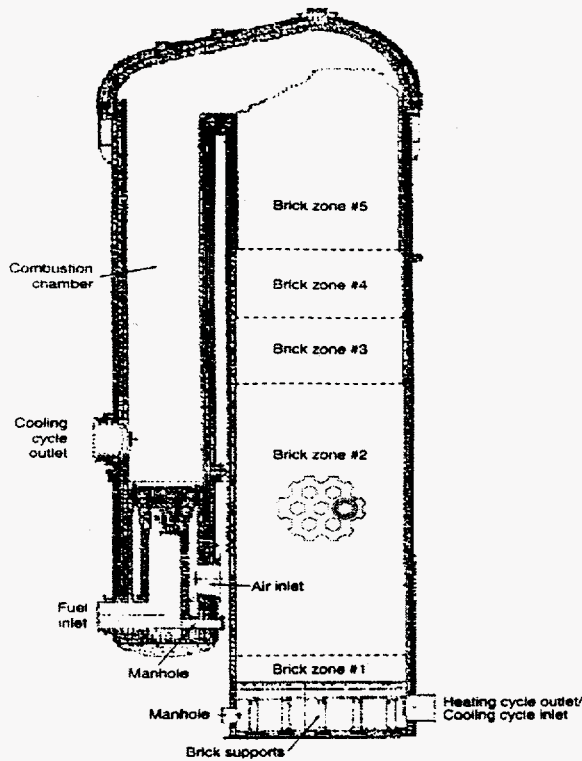


Figure 1: Blast furnace stove.

ducing the operating cost of the hot blast stoves is to minimize the amount of natural gas used to enrich the top gas. This minimization has to take into account the changing requirements in the blast air volume and temperature that must be achieved for proper blast furnace operation.

2 Process Model

The blast furnace stove is modeled by assuming that the gas channels in the checkers comprising the stove can be represented as thick walled tubes in which the gas flows through the center of the tubes heating or cooling the wall material. The outside wall of the tubes are assumed to be perfectly insulated. The tubes are divided into five zones each containing a different checker material. The top of the stove is comprised of silica checkers. The lower zones are comprised of mullite, super duty, high duty, and high alumina checkers respectively. The stove model geometry

is shown in Figures 2 and 3.

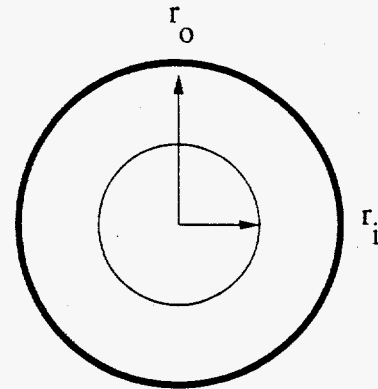


Figure 2: Stove model geometry top view.

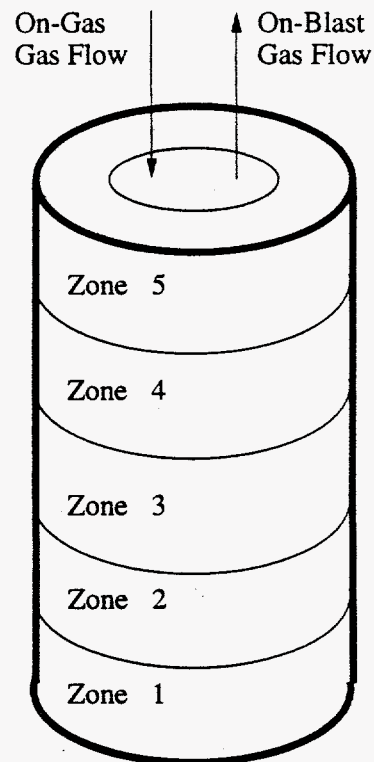


Figure 3: Stove model geometry side view.

The number of tubes used to represent the stove is the number of gas channels in the checkers. This value, denoted by N_c , is the same for each of the five zones and is specified by the stove manufacturer. The radius of the gas channel in the tube, r_i , is one half of the hydraulic diameter of the gas channels in the corresponding checker. The outside radius of the tube, r_o , is determined

from the total number of gas channels, N_c , the hydraulic diameter of the gas channel, D_h , the total mass and density of the checkers, m_n and ρ_n , and the length of the zone, L_n , in which the subscript n refers to the zone. These values are specified by the stove manufacturer for each zone.

$$r_o = \sqrt{\frac{m_n}{\pi \rho_n N_c L_n} + \frac{D_h^2}{4}} \quad (1)$$

2.1 Gas Model

The blast air and waste gas are modeled by an energy balance over the gas flowing through a single tube. Assuming the blast air and waste gas are ideal gases, no radial variation of the gas temperature, and no heat conduction in the gas in the axial direction results in the following PDE [1]

$$\rho_g C_{p,g} \left[\frac{\partial T_g}{\partial t} + v_g \frac{\partial T_g}{\partial z} \right] + v_g \frac{\partial P}{\partial z} = \frac{4h}{D_h} (T_g - T_w) \quad (2)$$

in which T_g is the gas temperature, v_g is the gas velocity, ρ_g is the gas density, $C_{p,g}$ is the gas heat capacity, P is the pressure, h is the gas-solid heat transfer coefficient, D_h is the hydraulic diameter of the gas channel, and T_w is the solid wall temperature.

The density of an ideal gas is determined as follows in which M_g is the average molecular weight.

$$\rho_g = \frac{M_g P}{RT_g} \quad (3)$$

For the on-blast cycle, the average molecular weight of air, corrected for the moisture injected into the blast air, is used. For the on-gas cycle, the molecular weight is determined from the computed waste gas composition which is discussed in the sequel.

The heat capacity of each of the components in the blast air and waste gas are determined by interpolating functions of the heat capacity vs. temperature data contained in the National Bureau of Standards Publication #564 on the thermal properties of gases [2]. The interpolating

function for each component is shown in Table 2 in Appendix A.

The gas velocity in the tubes is determined from the stove inlet mass flow rate, \dot{m}_{in} , the gas density, and the cross-sectional area of the tube assuming a uniform gas flow distribution through the channels in the checkers.

$$v_g = \frac{4\dot{m}_{in}}{\pi \rho_g N_c D_h^2} \quad (4)$$

For the on-gas cycle, the inlet mass flow rate is determined from the combustion air and mixed fuel gas flow rates. For the on-blast cycle, the blast air inlet mass flow rate depends on the amount of blast air flow by-passed to achieve the desired blast air temperature target. The inlet mass flow rate can be determined from an energy balance over the stove in which T_g^{targ} is the desired blast air temperature, T_g^{in} is the blast air inlet temperature, T_g^{out} is the temperature of the blast air exiting the stove before mixing, and \dot{m}_{total} is the total blast air mass flow rate.

$$\dot{m}_{in} = \left(1 - \frac{\int_{T_g^{targ}}^{T_g^{out}} C_{p,g} dT}{\int_{T_g^{in}}^{T_g^{out}} C_{p,g} dT} \right) \dot{m}_{total} \quad (5)$$

In order to determine the energy of expansion term in Eq. 2, the pressure profile in the tube is required. The inlet pressure during the on-gas cycle and the outlet pressure during the on-blast cycle are measured. Assuming that the pressure drop across the stove is due to frictional losses that can be modeled in the same manner as friction losses in a pipe results in the following relationship [1]

$$\frac{dP}{dz} = \frac{f \rho_g v_g^2}{2 D_h} \quad (6)$$

in which the friction factor f is determined from the following correlation by Jain [3].

$$\frac{1}{\sqrt{f}} = 3.4841 - 1.7372 \ln \left[\frac{2\epsilon}{D_h} + \frac{42.5}{Re^{0.9}} \right] \quad (7)$$

The equivalent sand roughness of the checker material, ϵ , is assumed to be similar to that of concrete. A value of $\epsilon = 0.02$ was determined from a

plot of equivalent sand roughness for commercial pipe surfaces [4].

The gas-solid heat transfer coefficient is comprised of a convective contribution and a gas-solid radiation contribution for the on-gas cycle only.

$$\text{on-gas: } h = h_c + h_r, \quad \text{on-blast } h = h_c \quad (8)$$

The contribution from radiation, h_r , is determined from a gas temperature correlation by Schofield *et al.* [5]. The convective contribution, h_c , is determined from a correlation for rough pipes by Bhatti and Shah [4]

$$\text{Nu} = \frac{(f/2)(\text{Re} - 1000)\text{Pr}}{1 + \sqrt{f/2} [(17.42 - 13.77\text{Pr}_t^{0.8})\sqrt{\text{Re}_\epsilon} - 8.48]} \quad (9)$$

with the values of the turbulent Prandtl number, Pr_t , and the roughness Reynolds number, Re_ϵ computed from the following relationships.

$$\text{Pr}_t = 1.01 - 0.99\text{Pr}^{0.36} \quad (10)$$

$$\text{Re}_\epsilon = \frac{\epsilon v_g}{\mu_g} \sqrt{\frac{f}{2}} \quad (11)$$

The Nusselt, Reynolds, and Prandtl numbers are defined as follows

$$\text{Nu} = h_c D_h / k_g$$

$$\text{Re} = D_h v_g \rho_g / \mu_g$$

$$\text{Pr} = C_{p,g} \mu_g / k_g$$

in which μ_g is the gas viscosity and k_g is the gas thermal conductivity.

The viscosity and thermal conductivity of the blast air and waste gas are required to determine the Nusselt, Reynolds, and Prandtl numbers. These properties as a function of temperature for each of the blast air and waste gas components are determined by interpolating functions of the data contained in the National Bureau of Standards Publication #564 on the thermal properties of gases [2]. The viscosity interpolating functions are presented in Table 3 and the thermal conductivity interpolating functions are presented in Table 4 in Appendix A. The viscosity of the blast air and waste gas is determined from the

pure component viscosities using the method of Wilke. The thermal conductivity is determined from the pure component thermal conductivities using the method of Mason and Saxena. These methods are outlined in Appendix B. The effect of the excess oxygen present in the waste gas is ignored in these calculations.

The temperature of the incoming blast air during the on-blast cycle is available from a process measurement. This value is used as the inlet temperature boundary condition for Eq. 2 during the on-blast cycle. The temperature of the combustion gases entering the top of the stove during the on-gas cycle is not measured. This value is determined by an energy balance over the fuel and combustion air and is used as the inlet temperature boundary condition during the on-gas cycle. The composition of the natural gas for the energy balance is taken as the nominal composition specified by the utility supplying the gas. The top gas composition is determined by a process analyzer. Since the top gas is scrubbed before being sent to the stoves, it is assumed to be saturated with water. The vapor pressure of water in the top gas is determined using the Antoine equation

$$\log(P_{\text{H}_2\text{O}}) = 0.154 - 32.258/(T - 45.150) \quad (12)$$

in which $P_{\text{H}_2\text{O}}$ is in psi and T is in K. The mixed fuel gas composition is determined from the composition and flow rate of each stream. The combustion air flow rate is determined by the desired excess oxygen concentration in the waste gas. This energy balance calculation is outlined in Appendix C.

Stove operating experience indicates that as the mixed fuel gas flow rate increases, a small amount of combustible components appear in the waste gas. This effect is caused by the burners that were designed for coke oven gas enrichment and produce less efficient natural gas combustion at high fuel gas flow rates. An adjustable parameter that specifies the fraction of natural gas combusted is included in the model to account for this effect. Determination of this value is based on an analyzer in the waste gas stream that measures the combustible components.

2.2 Solid Model

An energy balance over a single tube results in the following PDE for the solid wall material [1]

$$\rho_s C_{p,s} \frac{\partial T_s}{\partial t} - \frac{1}{r} \frac{\partial}{\partial r} \left(r k \frac{\partial T_s}{\partial r} \right) - k_s \frac{\partial^2 T_s}{\partial z^2} = 0 \quad (13)$$

in which T_s is the solid temperature, ρ_s is the solid density, $C_{p,s}$ is the heat capacity of the solid, and k_s is the thermal conductivity of the solid. The density for each of the five checker materials is specified by the stove manufacturer. The heat capacity and thermal conductivity for each of the five materials is specified as a function of temperature by the stove manufacturer.

Assuming heat transfer between adjacent zones with no heat loss, the boundary conditions for Eq. 13 in the axial direction are

$$k_n \frac{dT_s^n}{dz} \Big|_{z=L_n} = k_{n-1} \frac{dT_s^{n-1}}{dz} \Big|_{z=0} \quad (14)$$

in which k_n is the thermal conductivity of the checker material, T_s^n is the solid temperature, and L_n is the length of zone n . Assuming no heat conduction at the top of zone 5 and at the bottom of zone 1 results in the following axial boundary conditions for those zones.

$$\frac{dT_s^5}{dz} \Big|_{z=0} = \frac{dT_s^1}{dz} \Big|_{z=L_1} = 0 \quad (15)$$

Assuming the outside tube wall is perfectly insulated, the boundary conditions in the radial position are the following.

$$\begin{aligned} \frac{dT_s}{dr} \Big|_{r=r_o} &= 0 \\ \frac{dT_s}{dr} \Big|_{r=r_i} &= \frac{2h}{k_s r_i (r_o^2/r_i^2 - 1)} (T_g - T_s|_{r=r_i}) \end{aligned} \quad (16)$$

2.3 Simplified Solid Model

A simplification of Eq. 13 is to assume that the checkers behave as a lumped parameter thermal capacity in the radial direction. In this case, there is no radial variation of the solid temperature and

the single tube energy balance is expressed by the following two-dimensional PDE [1]

$$\rho_s C_{p,s} \frac{\partial T_s}{\partial t} - k_s \frac{\partial^2 T_s}{\partial z^2} = \frac{2h}{k_s r_i (r_o^2/r_i^2 - 1)} (T_g - T_s) \quad (17)$$

in which the axial boundary conditions are given in Eqs. 14 and 15.

The characteristic time for heat conduction in the checkers can be determined by the following ratio

$$\tau = \frac{(r_o - r_i)^2}{\alpha}, \quad \alpha = \frac{k_s}{\rho_s C_{p,s}} \quad (18)$$

in which α is the thermal diffusivity of the checker material. This value is on the order of 3 minutes for the checker materials in zones 1 through 3 and zone 5 at the normal operating temperature range of the stove. It is on the order of 5 minutes for checker material in zone 4. Since these values are an order of magnitude less than the cycle times in the stove, a lumped parameter model in the radial direction is expected to be adequate.

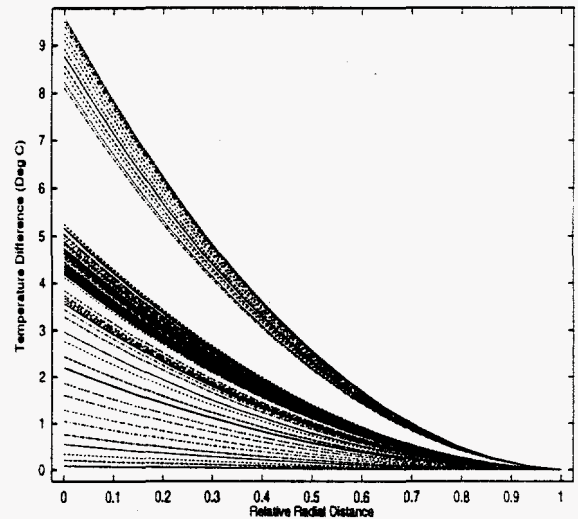


Figure 4: on-gas radial temperature variation.

Figures 4 and 5 present the normalized radial temperature profiles along the length of the stove at the end of a typical on-gas and on-blast cycle from the solution of Eq. 13. As shown in these figures, the maximum temperature variation in the

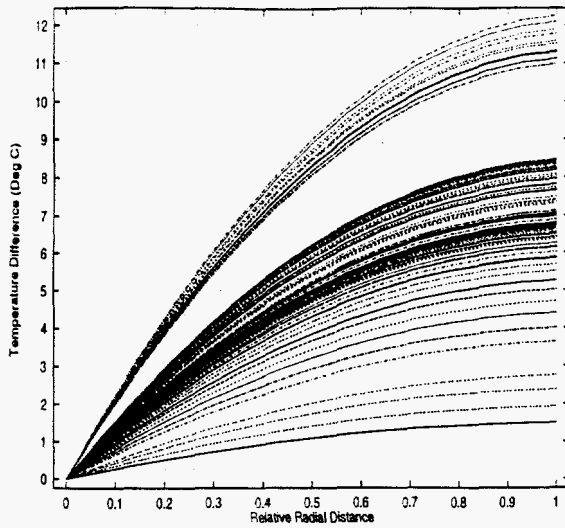


Figure 5: on-blast radial temperature variation.

radial direction is on the order of 10 C for a small fraction of the stove length. The majority of the stove length shows less than a 5 C variation for the on-gas cycle and less than a 7 C variation for the on-blast cycle. Comparison of the simulated axial temperature profile obtained from the simplified model in Eq. 17 with the radial averaged axial temperature profile obtained from Eq. 13 shows no significant difference. These simulation results confirm the conclusion based on the characteristic heat conduction times for the checker materials that a lumped radial model is adequate.

The advantage of the simplified model is a significant reduction in the computational effort required to solve the two-dimensional PDE in Eq. 17 as opposed to the three-dimensional PDE in Eq. 13. Since the model-based control algorithm requires a large number of successive model runs to determine the minimum fuel gas flow rate, the computation time of the model is an important consideration for the on-line implementation of the controller. For this reason, the simplified solid model is used in this work.

2.4 Pressurization and Blow-down

For blast air to enter the blast furnace, it must be above the blast furnace pressure. In order

to achieve the necessary blast air pressure, each stove is pressurized with air prior to the on-blast cycle. The energy removed from the checkers during this cycle is modeled by assuming the solid and gas temperatures after pressurization are in local thermal equilibrium along the tube length.

The equilibrium temperature profile, $T_{eq}(z)$, is determined by equating the energy removed from the solid tube wall to the energy necessary to heat the pressurization air. An energy balance at each axial node in the model results in the following equation

$$r_i^2 \int_{T_g^{in}}^{T_{eq}} \rho_g C_{p,g} dT = (r_o^2 - r_i^2) \rho_s \int_{T_{eq}}^{T_s^{init}} C_{p,s} dT \quad (19)$$

in which T_{eq} is the equilibrium solid and gas temperature at the axial node, T_g^{in} is the inlet pressurization air temperature, and T_s^{init} is the initial solid temperature determined from the previous on-gas cycle. The value of the equilibrium temperature is that which satisfies the equality in Eq. 19.

After an on-blast cycle is complete, the stove is returned to atmospheric pressure by venting the contents. The vented air leaves the combustion chamber of the stove by flowing through the checkerwork. The energy lost from the stove is modeled by the heat transfer from the tube wall to the gas vented from the combustion chamber that flows downward through the tubes.

Assuming an ideal gas, the mass flow rate of the gas leaving the combustion zone is

$$\dot{m}_{vent} = K_v m_i \sqrt{\frac{2}{\gamma - 1}} \left(\frac{P^*}{P}\right)^{\frac{1}{\gamma}} \left(\frac{m}{m_i}\right)^{\frac{\gamma+1}{2}} \sqrt{1 - \left(\frac{P^*}{P}\right)^{\frac{\gamma-1}{\gamma}}} \quad (20)$$

in which γ is the heat capacity ratio C_p/C_v , P is the stove pressure, P^* is the discharge pressure, m is the mass of gas in the stove, m_i is the initial mass of gas in the stove, and K_v is the discharge coefficient through the vent valve. The discharge coefficient is determined by matching

the computed and actual time to vent the stove. The minimum ratio of P^*/P is 0.538 due to sonic flow through the vent valve. The temperature of the gas leaving the combustion zone is determined by assuming isentropic expansion of an ideal gas and is computed by the following differential.

$$\frac{dP}{P} = \frac{\gamma}{\gamma - 1} \frac{dT}{T} \quad (21)$$

Since the thermal mass of the checkers is so much greater than that of the blast air involved in the pressurization and blow-down steps, the effect on the solid temperature is expected to be quite small. This conclusion is confirmed by the results of the preceding calculations. Although there are significant transient effects during these cycles, examination of the stove temperature data also confirms this conclusion. Therefore, the pressurization and blow-down steps are not considered in the stove model in order to reduce the computational requirements.

2.5 Model Results

The solution of the coupled PDE's in Eqs. 2 and 17 is performed using a Newton-Krylov technique to minimize the residuals of the finite volume discretized model equations. Further details on the solution technique are available in [6]. A comparison of the model predicted temperatures to those from a typical on-gas and on-blast cycle are presented in this section.

Figures 6 and 7 present the model predicted temperature profiles along the length of the stove at the end of an on-gas and on-blast cycle, respectively. The measured temperatures at the top of the stove, called the dome temperature, eleven meters from the top of the stove, called the interface temperature, and on the grid supports at the base of the stove, called the base temperature, are also included. As shown in the figures, the model predicts an almost linear temperature profile along the length of the stove for both cycles. These predictions are in accord with the available temperature measurements in the stove.

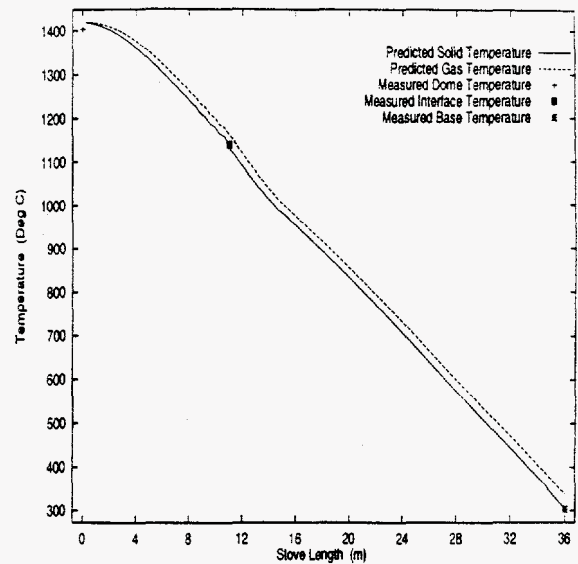


Figure 6: on-gas cycle temperature profile.

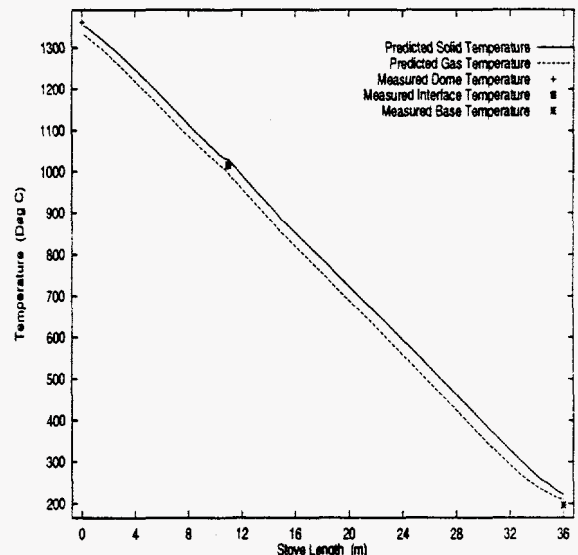


Figure 7: on-blast cycle temperature profile.

The model predicted dome, interface, and base temperatures for a single on-gas and on-blast cycle are presented in Figures 8, 9, and 10. The first fifty minutes in these figures represent the on-gas cycle, the next five minutes represent the pressurization cycle, the following thirty minutes represent the on-blast cycle, and the last five minutes are the blow-down cycle. These figures show good agreement with the measured temperatures.

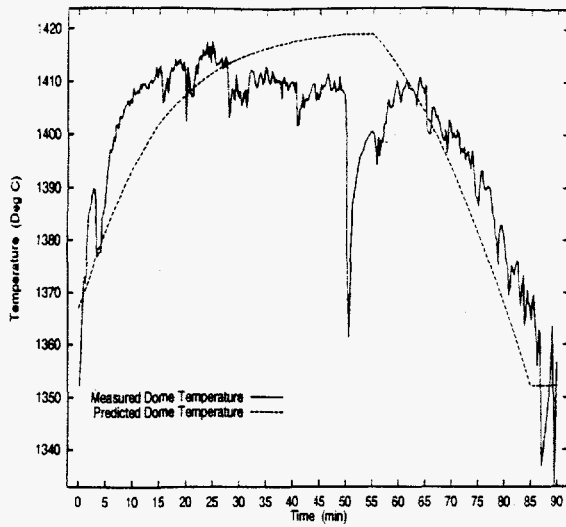


Figure 8: Dome temperature.

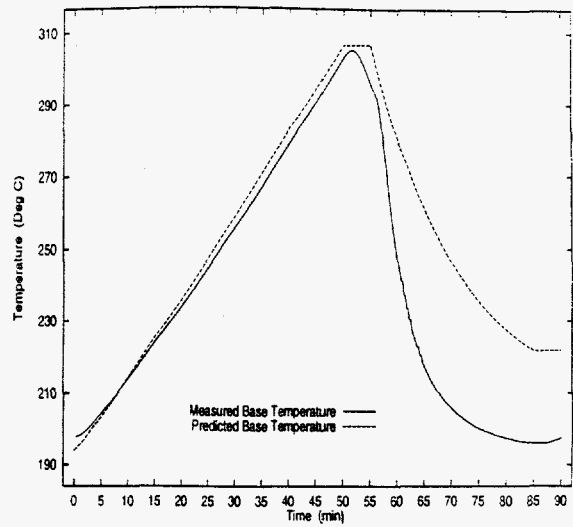


Figure 10: Base temperature.

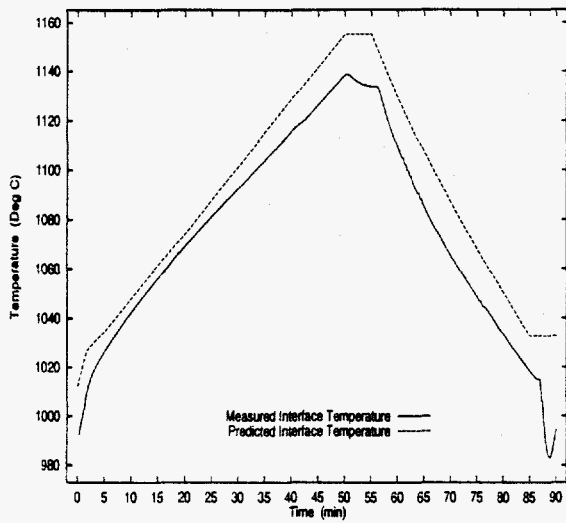


Figure 9: Interface temperature.

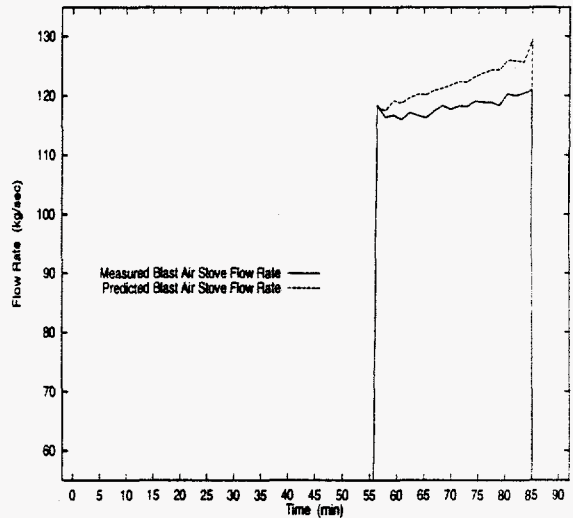


Figure 11: Blast air stove flow rate.

Figure 11 shows the model predicted blast air flow through the stove during the on-blast cycle. This flow is controlled by a by-pass valve that diverts part of the total blast air flow to the combustion chamber in order to control the blast air temperature. Temperature control is accomplished by mixing the cold diverted blast air with the hot blast air exiting the checkers. The measured value of this flow is based on a venturi meter reading corrected for the blast air temperature and pressure. The predicted value of this flow is determined from the model using Eq. 5.

3 Model-Based Control

The optimal operation of the blast furnace stove is that which uses the minimum amount of fuel necessary during the on-gas cycle to achieve the blast air flow rate and temperature requirements for the next on-blast cycle. This minimum represents the point where the cold blast air flow diverted to the combustion chamber to mix with the heated blast air is zero exactly at the end of the on-blast cycle. In practice, a small amount of

additional heat is put into the stove to ensure that the on-blast cycle requirements are met. This additional heat can be measured by the by-pass valve position at the end of the on-blast cycle. The by-pass valve position is determined in the model from the computed blast air flow rate entering the stove and a correlation between this blast air flow and the valve position

$$V^b = -2.189 + 2.716 \left(1 - \frac{\dot{m}_{in}}{\dot{m}_{total}}\right) - 0.056 \left(1 - \frac{\dot{m}_{in}}{\dot{m}_{total}}\right)^2 \quad (22)$$

in which V^b is the by-pass valve position, \dot{m}_{in} is the blast air flow rate through the stove, and \dot{m}_{total} is the total blast air mass flow rate.

The model-based controller implemented on the blast furnace stoves uses the stove model to adjust the mixed fuel gas flow rate during the on-gas cycle to achieve the desired blast air requirements while respecting temperature constraints and a minimum by-pass valve position constraint. The on-blast cycle calculation is included in order to determine the effect of the on-gas cycle fuel flow rate profile on the minimum temperature and by-pass valve position constraints. The maximum and minimum temperature constraints are the normal operating limits necessary to prevent thermal damage to the stoves. The exception is the minimum base temperature constraint that is set by the minimum waste gas temperature for pulverized coal drying. These constraints are summarized in Table 1. The controller also considers mixed fuel gas flow rate constraints. The maximum constraint of 30 m³/sec represents a mechanical vibration limit on the stoves. The minimum constraint is 18 m³/sec.

Location	Max Constraint	Min Constraint
Dome	1500 C	900 C
Interface	1200 C	800 C
Base	350 C	200 C

Table 1: Controller temperature constraints.

3.1 Model-Based Control Algorithm

The objective of the controller can be stated as the following optimization problem

$$\min_{F_i} \sum_{i=1}^5 F_i \quad (23)$$

$$\text{Subject to: } \begin{array}{l} F_{min} < F_i < F_{max} \\ T_{min}^d < T^d < T_{max}^d \\ T_{min}^i < T^i < T_{max}^i \\ T_{min}^b < T^b < T_{max}^b \\ V_{min}^b < V_f^b \end{array} \quad (24)$$

in which F_i are the mixed fuel gas flow rate profile for the on-gas cycle, T^d is the dome temperature, T^i is the interface temperature, T^b is the temperature of the grid supports at the base of the stove, V_f^b is the final by-pass valve position at the end of the on-blast cycle, and the maximum and minimum constraints are as previously specified.

The mixed fuel gas flow rate profile is comprised of five flow rates, F_1 through F_5 , each representing the mixed fuel gas flow rate for ten minutes of the on-gas cycle. This choice for the parameterization of the fuel flow rate is based on a compromise between the range of fuel flow rate profiles that can be considered by the controller and the solution time required by the optimization problem. The solution time, and the number of times the optimization fails, both increase exponentially with the number of decision variables. Since this optimization problem must be solved on-line, the profile was limited to five decision variables in order to reliably obtain a solution within a ten minute window.

The optimization problem for the controller is solved using a sequential, gradient-based, nonlinear optimization technique. The stove temperatures and mixing valve position are computed from the stove model using the current mixed fuel gas flow rate profile. The gradients of the objective function in Eq. 23 and each of the constraints in Eq. 24 are determined numerically from the model by perturbing the values of F_i around the current profile. Note that the minimum by-pass

valve position constraint is always active since reducing the fuel used during the on-gas cycle will decrease the amount of blast air by-passed during the on-blast cycle.

3.2 Controller Results

The model-predicted optimal fuel flow rate profile varies considerably from the constant profile typically implemented by the stove operators at Inland Steel. Figure 12 presents the constant fuel profile implemented during a typical on-gas cycle that resulted in a final by-pass value of 5 % at the end of the corresponding on-blast cycle. The optimal profile computed from the controller in Eqs. 23 and 24 results in a profile that uses the minimum amount of fuel at the beginning and end of the cycle while increasing the fuel usage in the middle of the cycle. The result is a predicted reduction of 9 vol% in mixed fuel gas use.

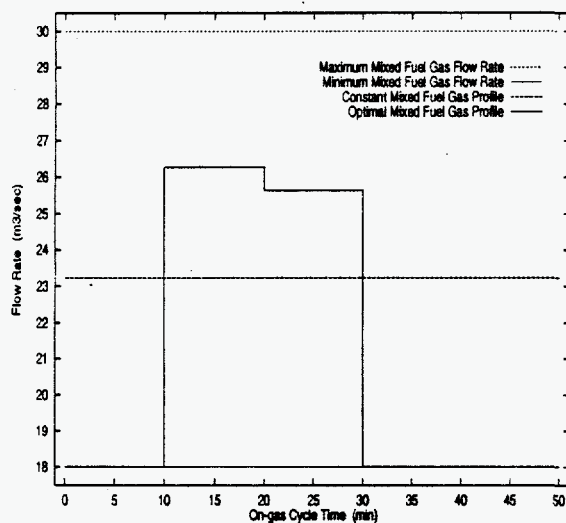


Figure 12: Optimal fuel flow rate profile.

A Pure Gas Physical Properties

Gas	$C_{p,g}(T)$ cal/gm-K
CO ₂	$0.3320 - 0.2173 \exp(-T/564.1)$
H ₂ O	$1.267 - 34.65/\sqrt{T} + 378.4/T$
N ₂	$0.2164 + 7.299e-5T - 1.361e-8T^2 - 947.2/T^2$
Air	$0.2566 - 1.211e-4T + 2.778e-7T^2 - 1.765e-10T^3 + 3.773e-14T^4$

Table 2: Heat capacity (T in deg K).

Gas	$\mu_g(T)$ cm/gm-sec
CO ₂	$-1.225e-4 + 3.107e-8T + 1.518e-5\sqrt{T}$
H ₂ O	$-7.962e-4 + 2.963e-5\sqrt{T} + 6.767e-3/\sqrt{T}$
N ₂	$-1.044e-4 - 2.656e-8T + 1.679e-5\sqrt{T}$
Air	$-5.769e-5 + 1.534e-5\sqrt{T} - 4.031e-4/\sqrt{T}$

Table 3: Viscosity (T in deg K).

Gas	$k_g(T)$ cal/cm-sec-K
CO ₂	$3.749e-5 + 3.559e-7 * T - 6.050e-6\sqrt{T}$
H ₂ O	$-3.977e-4 + 1.514e-5\sqrt{T} + 3.123e-3/\sqrt{T}$
N ₂	$-5.330e-5 - 8.804e-9T + 6.842e-6\sqrt{T}$
Air	$-8.278e-5 + 7.445e-6\sqrt{T} + 2.882e-4/\sqrt{T}$

Table 4: Thermal conductivity (T in deg K).

B Gas Mixture Properties

The viscosity of a gas mixture is estimated by the following relationship [7]

$$\mu_m = \sum_{i=1}^n \frac{y_i \mu_i}{\sum_{j=1}^n y_j \phi_{i,j}} \quad (25)$$

in which μ_m is the viscosity of the mixture, y_i is the mole fraction of component i , μ_i is the viscosity of pure component i , and the interaction parameter $\phi_{i,j}$ is computed by

$$\phi_{i,j} = \frac{(1 + (\mu_i/\mu_j)^{1/2}(M_j/M_i)^{1/4})^2}{\sqrt{8(1 + M_i/M_j)}} \quad (26)$$

with M_i the molecular weight of component i .

The thermal conductivity of a gas mixture is estimated by the following relationship [7]

$$k_m = \sum_{i=1}^n \frac{y_i k_i}{\sum_{j=1}^n y_j \alpha \phi_{i,j}} \quad (27)$$

in which k_m is the mixture thermal conductivity, y_i is the mole fraction of component i , k_i is the thermal conductivity of pure component i , $\phi_{i,j}$ is the interaction parameter shown in Eq. 26, and $\alpha = 0.85$.

C Combustion Temperature

The calculation of the combustion temperature for the on-gas cycle is performed by an adiabatic energy balance over the combustion zone. The inlet composition of the fuel/air mixture to the combustion zone is determined from the composition and ratios of the natural gas, top gas, and combustion air streams. The top gas composition is available on a dry basis from a process analyzer. The water content of the top gas is computed from the top gas temperature measurement assuming the gas is saturated with water using Eq. 12. The water content of the combustion air is determined from the relative humidity. Representative natural gas, top gas, and combustion air compositions are shown in Table 5.

Stream	Component	mole fraction
Natural Gas	CH ₄	0.805
	C ₂ H ₆	0.182
	N ₂	0.013
Top Gas	CO	0.240
	H ₂	0.034
	CO ₂	0.226
	N ₂	0.459
	O ₂	0.002
	H ₂ O	0.039
Air	O ₂	0.206
	N ₂	0.774
	H ₂ O	0.020

Table 5: On-gas inlet stream compositions.

The ratio of natural gas to top gas in the mixed fuel gas stream sent to the burners is set by a mixed fuel gas heating value controller. The heating value of the top gas typically ranges from 80–90 BTU/cuft. The typical target heating value of the mixed fuel gas ranges from 145–160 BTU/cuft resulting in a natural gas fraction of the mixed fuel gas on the order of 7 vol%. The natural gas fraction of the mixed fuel gas in the model is computed from the composition and the heating value target. The combustion air flow rate to the burners is set by an excess oxygen controller that maintains the excess oxygen in the waste gas at a nominal target of 1.2 vol%. The combustion air to mixed fuel gas ratio in the model is computed using the waste gas excess oxygen target.

The combustion temperature is determined from the following equality

$$\int_{T_{ref}}^{T_g^{in}} \left(\sum_{i=1}^{n_{in}} x_i C_{p,g,i} dT \right) + \sum_{i=1}^{n_{in}} x_i \Delta H_{v,i} = \int_{T_{ref}}^{T_g^{comb}} \left(\sum_{i=1}^{n_{out}} x_i C_{p,g,i} dT \right) \quad (28)$$

in which T_g^{comb} is the combustion temperature, T_g^{in} is the inlet gas temperature, T_{ref} is the reference temperature, x_i is the mass fraction for component i , $C_{p,g,i}$ is the gas heat capacity for component i , $\Delta H_{v,i}$ is the lower heating value for

component i , $n_{in} = 8$ is the number of components in the fuel gas/combustion air inlet stream, and $n_{out} = 4$ is the number of components in the waste gas outlet stream. The heat capacities as a function of temperature used in the integral of the inlet components and the heating values are taken from [8]. Note that $\Delta H_{v,i} = 0$ for the noncombustible inlet components. The reference temperature is 25 C. The heat capacities as a function of temperature used in the integral of the outlet components are taken from Table 2. Since noncombusted hydrocarbons are present at the ppm level, they are not considered in the waste gas. Brent's method [9], a single-variable search technique, is used to determine the combustion temperature from the integrated form of Eq. 28.

Thermophysics and Heat Transfer Conference, 1998.

References

- [1] R. B. Bird, W. E. Stewart, and E. N. Lightfoot. *Transport Phenomena*. Wiley, New York, 1960.
- [2] J. Hilsenrath, C. W. Beckett, W. S. Benedict, L. Fano, H. J. Hoge, J. F. Masi, R. L. Nuttall, Y. S. Touloukian, and H. W. Woolley. Tables of thermal properties of gases. Technical Report 564, National Bureau of Standards, 1955.
- [3] A. K. Jain. Accurate explicit equation for friction factor. *ASCE J. Hydraullic Div.*, 102:674-677, 1976.
- [4] M. S. Bhatti and R. K. Shah. Turbulent and transition flow convective heat transfer in ducts. In S. Kakac, R. K. Shah, and W. Aung, editors, *Handbook of Single-Phase Convective Heat Transfer*, New York, 1987. Wiley.
- [5] J. Schofield, P. Butterfield, and P. A. Young. Hot blast stoves. *J. Iron and Steel Inst.*, 39:229-240, 1961.
- [6] J. W. Howse, G. A. Hansen, D. J. Cagliostro, and K. R. Muske. Implicit Newton-Krylov methods for modeling blast furnace stoves. In *Proceedings of the AIAA/ASME Joint*

- [7] R. C. Reid, J. M. Prausnitz, and B. E. Poling. *The Properties of Gases and Liquids*. McGraw-Hill, New York, 4th edition, 1987.
- [8] V. M. Faires. *Thermodynamics*. MacMillan, New York, 4th edition, 1962.
- [9] W. H. Press, S. A. Teukolsky, W. T. Vetterling, and B. P. Flannery. *Numerical Recipes in C*. Cambridge University Press, 2nd edition, 1996.